POLYETHYLENE TEREPHTHALATE (PET) COATED WITH CHITOSAN AND CYCLOSPORINE A LAYERS AS A POTENTIAL STENT MATERIAL AND DRUG-DELIVERY SYSTEM

Klaudia Szafran[1,a], Małgorzata Jurak[1,b,*], Robert Mroczka[2,c], Katarzyna Pastuszak[1,d], Agnieszka Ewa Wiącek[1,e]

[1] – Department of Interfacial Phenomena, Institute of Chemical Sciences, Faculty of Chemistry, Maria Curie-Skłodowska University, Maria Curie-Skłodowska 3 Sq., 20-031 Lublin, Poland
[a] – ORCID: 0000-0002-0152-0839, [b] – ORCID: 0000-0002-5365-7677,
[d] – ORCID: 0009-0001-9682-0809, [e] – ORCID: 0000-0002-7425-9694
[2] – Department of Chemistry, Laboratory of X-Ray Optics, Faculty of Medicine, The John Paul II Catholic University of Lublin, Konstantynów 1J, 20-708 Lublin, Poland
[c] – ORCID: 0000-0001-9633-9188
[*]corresponding author: malgorzata.jurak@mail.umcs.pl

Abstract

The aim of this paper was to design, prepare and characterise chitosan (Ch) and cyclosporine A (CsA) mixed films deposited on a plasma-activated polyethylene terephthalate (PET) polymer surface to be used as a cover for implantable blood vessel stents. The PET polymer coated with Ch and CsA layers was immersed in simulated body fluid (SBF) to examine how the obtained layers can behave in the environment of human body fluids. Time-of-flight secondary ion mass spectrometry was employed to determine the chemical composition of the deposited films and to analyse the spatial distribution of molecules on the PET surface. The results showed the controlled release of CsA from the chitosan matrix. It can be concluded that the modification of the PET polymer with layers of chitosan and CsA has great application potential in the tissue engineering as a biocompatible stent of blood vessels with therapeutic properties.

Keywords: *chitosan, CsA, PET, air plasma, Langmuir–Blodgett technique, mass spectrometry*

Received: 28.02.2024
Accepted: 20.05.2024

1. Introduction

In recent decades, biomaterials used as implants have gained great importance in regenerative medicine and tissue engineering. Besides properties such as biocompatibility and non-toxicity [1–3], newly designed biomaterials should meet more advanced requirements. One of the unique features can be the ability to deliver and release the drugs in a controlled way. Among the most commonly used materials for the production of blood vessel stents or its coverage is polyethylene terephthalate (PET, Figure 1a) [4, 5]. Despite the appropriate chemical resistance, elasticity and fibre strength, PET causes a negative immune response when it comes in contact with living cells, which can result in rejection of the implant [4]. Thus, coating PET with a natural polymer like chitosan (Figure 1b) can significantly increase its biocompatibility.

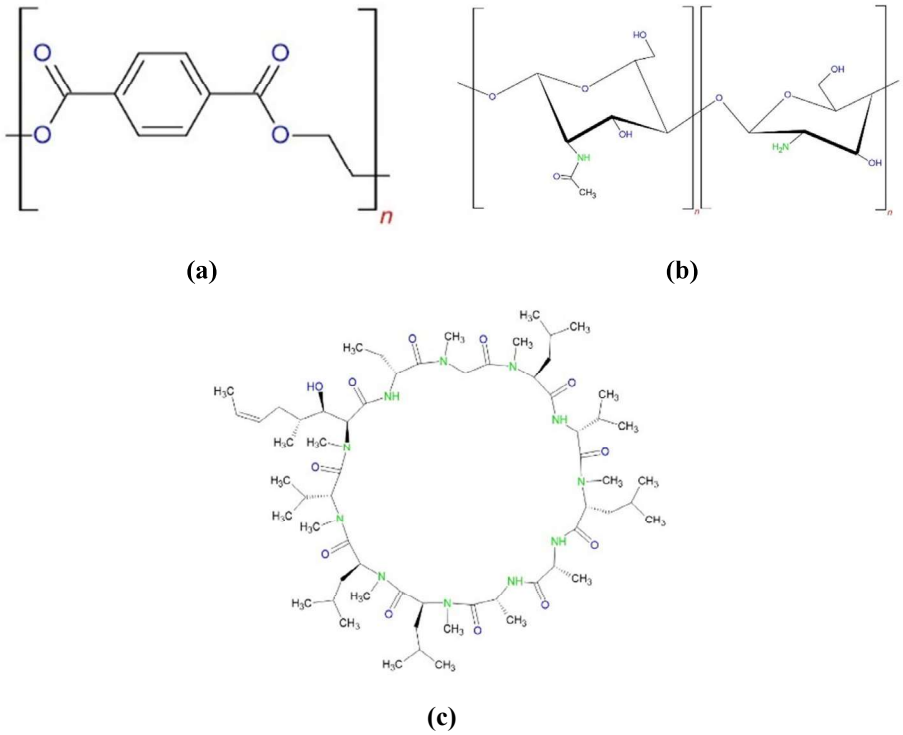

Figure 1. Chemical structure of (a) polyethylene terephthalate (PET), (b) chitosan and (c) cyclosporine A.

Chitosan is a polysaccharide consisting of *N*-acetyl-glucosamine and D-glucosamine monomers [6]. It occurs naturally: it is produced by fungi but it can also be obtained by deacetylation of chitin from shellfish shells [7]. Depending on the conditions of this process, chitosan with a different degree of deacetylation as well as physicochemical properties is obtained. In addition, chitosan is biocompatible and biodegradable, which results in production of oligosaccharides that are harmless to humans and can be easily processed by metabolic pathways and/or excreted by the body [8, 9]. Furthermore, chitosan has mucoadhesive, antimicrobial, antiviral and antifungal properties [6]. Additionally, chitosan is used to design

controlled drug-release systems. This is possible due to the simplicity of changing its properties by the pH, temperature or ionic strength of the solvent adjustments [10, 11]. Therefore, the use of chitosan as a coating of the biomaterial can allow for the delivery of a drug directly to the desired place in the body. Moreover, such coatings slow down the degradation rate and modulate cellular responses and the local release of growth factors from the biomaterial surface. As a result, postoperative complications are minimised [12, 13]. This property is extremely important in the case of strongly hydrophobic substances, whose absorption from the gastrointestinal tract is reduced significantly. However, in the bloodstream, positively charged chitosan ($-NH_3^+$) can interact with negatively charged platelets, provoking clot formation [14]. Thus, the simultaneous use of chitosan with the other substances seems to be appropriate to reduce its charge density and thus make it less thrombogenic.

One of the drugs frequently utilised after placing a biomaterial in the human body is cyclosporine A (CsA, Figure 1c); this cyclic polypeptide consisting of 11 amino acids has strong immunosuppressive properties. CsA works by inhibiting T lymphocyte–dependent immune reactions without affecting bone marrow cells. It also exhibits antifungal, anti-inflammatory and antiparasitic activities [15–17]. CsA is able to permeate membranes via passive diffusion. This process is associated with changes in the CsA conformation, which strictly depends on the polarity of the surrounding medium [18, 19]. However, due to its high molecular weight (1202.61 Da) and the possibility of forming intramolecular hydrogen bonds, CsA is poorly soluble in water and body fluids. Therefore, there are problems with the bioavailability and biocompatibility of CsA, which make oral administration of the drug ineffective (20%–50%) [15–17]. Accordingly, designing a controlled drug-release system that is simultaneously a biomaterial coating could eliminate this disadvantage. Figure 2 illustrates schematically a PET stent coated with chitosan and CsA films placed in a blood vessel.

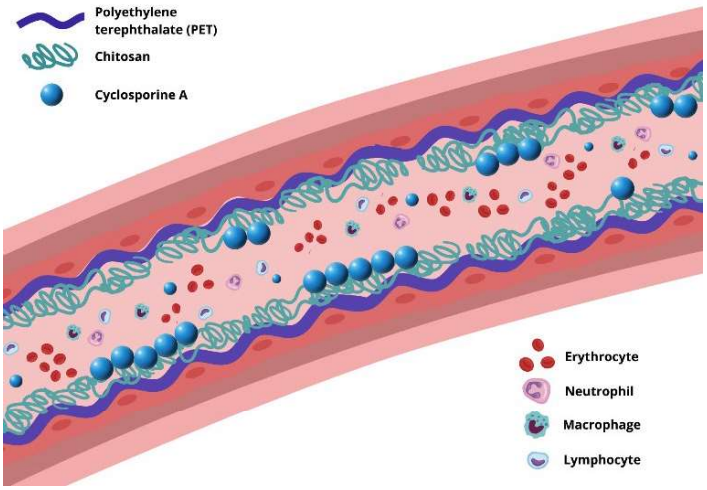

Figure 2. Scheme of the blood vessel with a polyethylene terephthalate stent coated with chitosan and cyclosporine A layers.

De Campos et al. [20] proved that chitosan nanoparticles form a support for CsA and can be applied in ophthalmology. This is possible due to the hydrogen bonds that form between amino groups of chitosan and amide groups of CsA. Additionally,

both acetylated and deacetylated units of chitosan are capable of forming hydrogen bonds [21]. Besides, chitosan membranes loaded with CsA as possible vehicle for local administration of drugs in breast cancer treatment have also been described [22]. It should be emphasised that chitosan increases the permeability of the epithelial membrane that promotes the stability of the drug at the absorption site and its paracellular transport [23].

The aim of this study was to elaborate novel chitosan-based biocoatings for PET stents which can be used for drug delivery, local release and absorption into the blood. For this purpose, the Langmuir–Blodgett technique was employed to prepare CsA monolayer at the chitosan/air interface and deposit it onto the air plasma–activated PET (PET_{air}) support. Additionally, previously prepared samples were immersed in simulated body fluid (SBF). By contacting the biomaterial with a solution containing ions present in body fluids, it was possible to examine how the obtained coatings would behave after grafting them in the human body. Afterwards, the chemical composition of the polymer coating was examined by the time-of-flight secondary ion mass spectrometry (TOF-SIMS).

2. Materials and Methods

2.1. Materials

Plates (20 × 30 × 3 mm^3) were cut from commercially available PET (Bayer Material Science, Germany) and used as a solid support. A 0.1 mg ml^{-1} chitosan solution was prepared by dissolving an appropriate amount of chitosan (molecular weight 100,000–300,000, degree of deacetylation 82% ± 2%, Acrōs Organics, Sweden) in 0.1% acetic acid diluted from concentrated acetic acid (99.5%–99.9%, Avantor Performance Materials Poland S.A., Poland). Additionally, CsA (≥ 99%, Alfa Aesar, Germany) was dissolved in chloroform:methanol mixed in a 4:1 ratio (v:v) to obtain a 1 mg ml^{-1} concentration (chloroform 99.8%, Macron Fine Chemicals, Avantor Performance Materials Poland S.A., and methanol ≥99.9%, Fluka, Sweden). SBF was prepared according to the procedure described by Kokubo et al. [24]. All used chemicals – NaCl, Na_2CO_3, $Na_2HPO_4 \times 12H_2O$, $MgCl_2 \times 6H_2O$, $CaCl_2$ (POCh Poland), KCl, Na_2SO_4 (Chempur, Poland) and tris(hydroxymethyl)aminomethane ($NH_2C(CH_2OH)_3$, Sigma-Aldrich, USA) – were dissolved in Milli-Q water with resistivity of 18.2 MΩ cm (Milli-Q Plus 185 system, Millipore, USA).

2.2. Methods

The PET plates were cleaned as described previously [25, 26]. Then, the plates were activated by a low-temperature and low-pressure (0.20 mbar) air plasma (Plasma type system, Diener Electronic, Germany) for 1 min. Immediately after modification, the PET plates were immersed in the chitosan subphase filling the Langmuir–Blodgett trough (KSV 2000 Standard, Finland), which had been purified with acetone (99.5%, Avantor Performance Materials S.A. Poland), methanol and deionised water. The surface tension was measured by the Wilhelmy plate method with an accuracy of 0.1 mN m^{-1}. Subsequently, the proper volume of CsA solution was spread onto the chitosan subphase. After solvent evaporation, symmetrical compression with a constant speed of 20 mm min^{-1} was performed to achieve a surface pressure of 10 mN m^{-1} at which the CsA monolayer was found to be the most stable on the liquid subphase [26, 27]. Immediately after reaching the target pressure, the CsA monolayer was transferred onto the PET plate during its withdrawal from the subphase towards the air. Then, the PET substrate with the deposited Langmuir–Blodgett layers was dried to remove traces of water and placed in a dark glass

desiccator before the next stages of the experiment. Afterwards, the samples were immersed in SBF for 3, 10 or 30 min. Subsequently, TOF-SIMS was performed. The modified PET substrates were placed in the ultra-high vacuum chamber of the TOF-SIMS.5 instrument (ION-TOF GmbH, Germany). The primary ion source of bismuth ions (Bi^+) was utilised at 30 keV and corresponded to the 1.0 pA primary beam current in the spectrometry mode where the scanning area of the secondary ions was 200 × 200 μm^2 with 256 × 256 pixels. All measurements were performed under static positive conditions (dose < 1 × 10^{12} ions cm^{-2}). To neutralise the charge left on the surface, an electron flood gun (20 eV) and a surface potential (U = −360 V) were applied. The spectra were calibrated based on the positions of $(CH_3)^+$, $(C_2H_3)^+$ and $(C_2H_5)^+$. The intensity of each fragment was normalised to the total intensity.

3. Results and Discussion

The design of biocompatible coatings for implants that can be used simultaneously as a controlled drug-release system requires one to examine the chemical composition, which is one of the main properties influencing the host body's immune response [2]. In the present study, the PET surface was activated by plasma leading to generation of new functional groups containing oxygen, nitrogen and carbon (-OH, C-O, O=C-O, C=O, and N-CO-N). Their presence was confirmed by X-ray photoelectron spectroscopy (XPS) from our previous study [26] as wellas those studies from other researchers [28–30]. Subsequently, the CsA monolayer was deposited onto the plasma-activated PET (PET_{air}) support by using the Langmuir–Blodgett technique from the chitosan/air interface. This process leads to the formation of new bonds between the activated polymer surface and chitosan [26]. Then, TOF-SIMS was conducted before and after immersion of the PET plates with the deposited chitosan and/or CsA layers in SBF for different periods of time. This technique allows one to determine the chemical structure and fragmentation patterns of molecules based on the mass to charge (*m/z*) ratio of the molecular fragments formed during ionisation [31]. Due to the fact that only single-charge mass fragments are produced when ionisation is carried out using a bismuth source in the TOF-SIMS spectrometer chamber, the m/z value corresponds practically to the mass of the formed ion. The TOF-SIMS spectra obtained for the mass range of the most characteristic fragments of CsA and chitosan deposited onto the PET_{air} support, along with the whole *m/z* range from 0 to 1300, are presented in Figure 3.

Table 1 summarises the *m/z* assignment and identification of these fragments. Figures 4 and 5 show the distributions of the fragments. The most prominent ions identified for the single CsA monolayer are *m/z* = 100 $(C_6H_{14}N)^+$ (Figure 4a), pseudomolecular *m/z* = 1172 $(C_{61}H_{108}N_{10}O_{12})^+$ and molecular ion *m/z* = 1202 $(C_{62}H_{112}N_{11}O_{12})^+$ (Figure 4b); these findings are consistent with our previous papers [25, 26, 32]. We also noted the pseudomolecular ion with *m/z* = 1188 $(C_{62}H_{112}N_{10}O_{12})^+$. The fragments with *m/z* = 1172 and 1188 come from the molecular ion (*m/z* = 1202) by subtraction of NH_3 and N, respectively. Based on the TOF-SIMS mass spectra, they showed significantly higher intensity (Figure 3c). Thus, we selected the molecular ion (*m/z* = 1202) as the primary meaning and the most intense fragment (*m/z* = 1172) for further analysis; this choice provided better statistical results. The high-mass fragments are typical of the mass patterns of polymers or oligomers (Figure 3c).

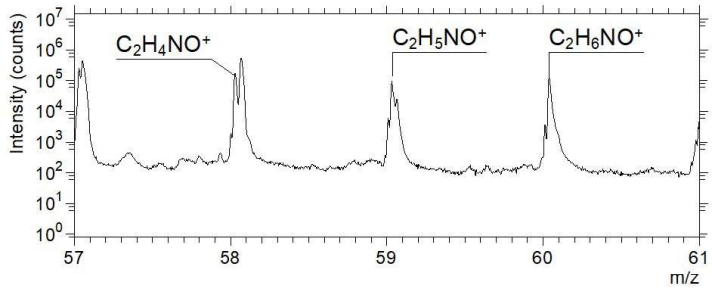

(a)

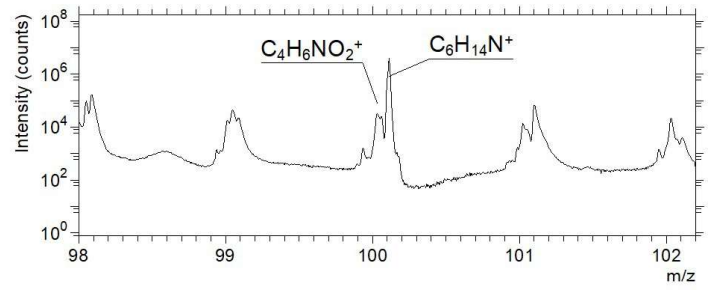

(b)

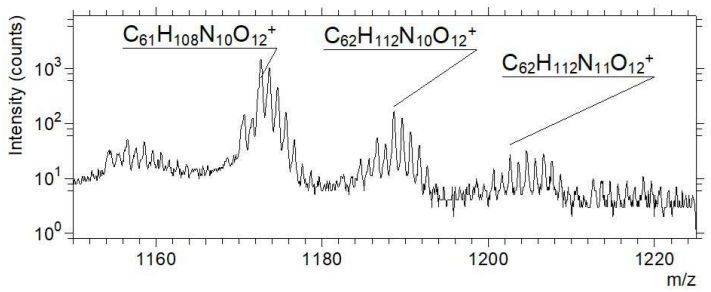

(c)

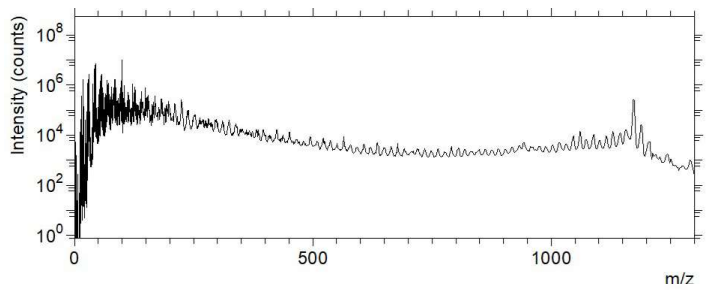

(d)

Figure 3. The time-of-flight secondary ion mass spectra (with a logarithmic scale) for mass range (*m/z*) (a) from 57 to 61 (peaks characteristic of chitosan), (b) from 98 to 102 (peaks characteristic of chitosan and cyclosporine A), (c) from 1150 to 1224 (the high-mass fragments that results from cyclosporine A) and (d) for the entire mass range from 0 to 1300.

It should be emphasised that the molecular ion is the basic ion identifying a given component of the monolayer and serves as an indicator of its order; it is closely related to the arrangement and/or inclination of the molecules. It is defined as a charged molecule that is formed as a result of ionisation by donating one electron (a positive molecular ion) or, much less often, by taking one electron (a negative molecular ion). Its mass is equal to the molecular weight of the tested compound. Meanwhile, a pseudomolecular ion is created by removing two oxygen or hydrogen atoms from the molecular ion or by adding a foreign metal from the environment.

Table 1. The most characteristic positive fragments in the time-of-flight secondary ion mass spectra obtained for the chitosan (Ch) and cyclosporine A (CsA) layers.

Assignment	m/z	Identification	Reference
$(C_6H_{14}N)^+$	100	CsA	[25, 26, 32]
$(C_{61}H_{108}N_{10}O_{12})^+$ $(CsA–NH_3)^+$	1172	CsA pseudomolecular ion	[25, 26, 32]
$(C_{62}H_{112}N_{10}O_{12})^+$ $(CsA+H–N)^+$	1188	CsA pseudomolecular ion	This study
$(C_{62}H_{112}N_{11}O_{12})^+$ $(CsA+H)^+$	1202	CsA molecular ion	[25, 26, 32]
$(C_2H_4NO)^+$	58	Ch	[26, 33]
$(C_2H_5NO)^+$	59	Ch	[26]
$(C_2H_6NO)^+$	60	Ch	[34]
$(C_4H_6NO_2)^+$	100	Ch	[34]

Other researchers have also identified secondary ions assigned to CsA by TOF-SIMS. Muddiman et al. [35, 36] quantified the $(CsA+Na)^+$ *m/z* = 1225 and $(CsA+Ag)^+$ *m/z* = 1309 fragments on an etched silver substrate with a mass resolution of 8000. In addition, Nicola et al. [37] identified the $(CsA+H)^+$ *m/z* = 1202 and $(CsA+Ag)^+$ *m/z* = 1309 fragments for the CsA layer deposited on silver support previously covered with a cocaine layer. Finally, Biddulph [38] identified the following CsA fragments: $(M+H)^+$ *m/z* = 1202, *m/z* = 100, (leucine) *m/z* = 86, (valine) *m/z* = 72, (alanine) *m/z* = 44, (glycine) *m/z* = 30 and *m/z* = 15. They were yielded by the Au^{3+} primary ion with a relative intensity of 394.5×10^{-5}, 3207.0×10^{-5}, 751.9×10^{-5}, 340.5×10^{-5}, 1205.0×10^{-5} and 81.4×10^{-5}, 37.5×10^{-5}, respectively. For comparison, in the present study the relative intensity of the fragments *m/z* = 100, 1172 and 1202 before immersion in SBF was 0.1×10^{-4}, 8.5×10^{-4} and 1.2×10^{-5}, respectively (Figure 4). Mass resolution was 12652 for the *m/z* = 1172 fragment and 9348 for the *m/z* = 1202 fragment. The former fragment resulted from extraction of *m/z* = 30, which presumably corresponds to C_2H_6.

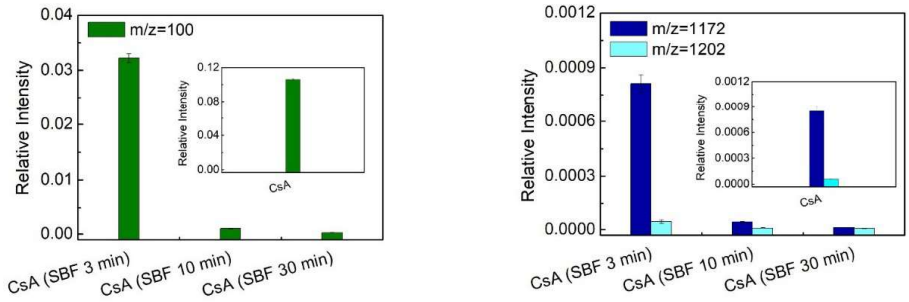

Figure 4. Distribution of the (a) cyclosporine A *m/z* = 100 fragment and the (b) *m/z* = 1172 and 1202 fragments for the air plasma–activated polyethylene terephthalate (PET_{air})/chitosan (Ch)/cyclosporine A (CsA) surface before and after immersion in simulated body fluid (SBF) solution for different periods of time.

As can be seen in Figure 4a,b, the relative intensity of the characteristic CsA fragments was the greatest for the deposited CsA monolayer before immersion in SBF. This correlated with the largest surface coverage. Moreover, the presence of the molecular and pseudomolecular ions confirmed that the obtained monolayer was well ordered. As a result of interactions with the primary ion beam (Bi^+ or Bi^{3+}), the molecules in such a layer are subject to much less fragmentation, which favours high molecular ion efficiency [34]. In other words, in the well-ordered and packed monolayer, the probability of yielding the molecular or pseudomolecular ions (*m/z* = 1170 and 1202) increases significantly. This can be justified by the number of molecules and the intermolecular interactions. Specifically, at very low surface coverage, the CsA molecules are loosely arranged and the interactions between them can be neglected (like in a gas phase) or can be very low (like in a liquid state). Under these circumstances the fragmentation of isolated molecules by primary the Bi^{3+} beam is very high. Hence, the probability of desorption of CsA in their original, unfragmented form is close to zero. When the monolayer is more tightly packed, the intermolecular interactions allow some portion of CsA to be desorbed from the substrate in the unfragmented form and further to be extracted to the analyser chamber of the TOF-SIMS instrument and identified by the detector.

Furthermore, as the CsA monolayer was deposited onto the PET_{air}/chitosan surface, the signal intensity coming from the characteristic fragments of chitosan was the smallest (Figure 5). After immersion of the sample in SBF for 3 min, the relative intensity of the $(C_6H_{14}N)^+$ ion was 3 times smaller with almost the same intensities of the molecular $(C_{62}H_{112}N_{11}O_{12})^+$ and pseudomolecular $(C_{61}H_{108}N_{10}O_{12})^+$ ions (Figure 4b). This can be related to some changes in the CsA molecular organisation due to contact with the liquid. The occurrence of molecular ions proves that CsA monolayer is still present at the PET_{air}/chitosan surface. When the PET_{air}/chitosan/CsA sample was immersed in SBF for a longer time, the relative intensity of CsA molecular ions decreased (Figure 4b). At very low surface coverage with CsA (immersion times of 10 and 30 min), the molecules are too far from each other and thus do not interact. Consequently, the probability of yielding the molecular ion during sputtering by the primary Bi^+ ion beam is strongly diminished. This phenomenon has been well reported in the literature [25, 26, 34, 39]. Thus, the obtained results demonstrate that the packed and ordered CsA monolayer

structure is not retained and most of the CsA molecules can be desorbed into the bulk phase. The intensity of $(C_6H_{14}N)^+$ ion with *m/z* = 100 shows similar behaviour (Figure 4a). This affirms that CsA molecules are still present at the surface.

In the time-of-flight secondary ion mass spectra, the chitosan layer was identified in the form of $(C_2H_4NO)^+$, $(C_2H_5NO)^+$ and $(C_2H_6NO)^+$ (Table 1), consistent with our previous study [26]. Figure 5 shows the intensity distribution of these chitosan fragments. Of note, we obtained the *m/z* = 100.04 fragment assigned to $(C_4H_6NO_2)$+, which is characteristic of chitosan [34]. Despite the similar *m/z* ≈ 100 values, we could distinguish that peak from the most intense CsA fragment $(C_6H_{14}N)^+$, namely *m/z* = 100.10, due to high mass resolution (> 8000). The relative intensity of $(C_4H_6NO_2)^+$ was 1.46×10^{-3}, 5.2×10^{-4}, 2.2×10^{-4} and 3×10^{-4} for samples before immersion in SBF, and after immersion in SBF for 3, 10 and 30 min, respectively. The intensity of this chitosan fragment was significantly lower compared with the others (*m/z* = 58, 59 and 60, Figure 5). We expected that the intensity would increase after immersion in SBF similarly to *m/z* = 60. Due to the fact that the *m/z* = 60 fragment demonstrated the proper distribution (with a significant increase in intensity after immersion), we used it as an indicator of the chitosan layer. On the other hand, owing to the low intensity and atypical behaviour after immersion of the *m/z* = 100.04 fragment, we did not consider it further.

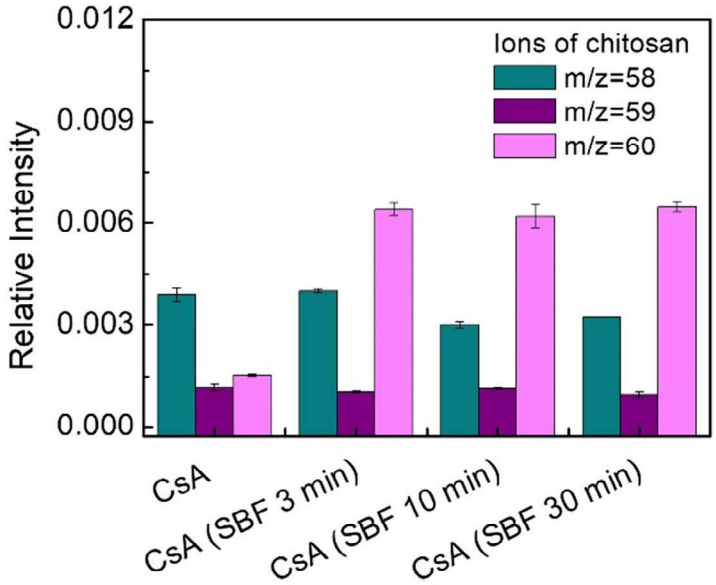

Figure 5. Distribution of the chitosan *m/z* = 58, 59 and 60 fragments for the air plasma–activated polyethylene terephthalate (PET_{air})/chitosan (Ch)/cyclosporine A (CsA) surface before and after immersion in simulated body fluid (SBF) for different periods of time.

As shown in Figure 5, the relative intensity of the *m/z* = 58, 59 and 60 fragments varied depending on the nature of deposited layer and possible post-treatment method. For the untreated Ch/CsA layer, the $(C_2H_4NO)^+$ fragment (*m/z* = 58) showed the highest intensity. On the other hand, the $(C_2H_5NO)^+$ and $(C_2H_6NO)^+$ intensities are roughly similar and two times lower than that of the $(C_2H_4NO)^+$ ion. There were similar results in the recent studies [26, 33, 34]. After immersing the Ch/CsA layer in SBF for 3 min,

the relative intensity of the *m/z* = 58 and 59 fragments remained unchanged. Meanwhile, the relative intensity of the $(C_2H_6NO)^+$ fragment (*m/z* = 60) increased more than 3 times, which corresponds to a decrease in the amount of CsA on the surface (lower intensity of the CsA fragment with mass *m/z* = 100). On the other hand, the intensity of the CsA molecular ions is the same. These results suggest that orientation of the CsA molecules is very likely preserved at even lower surface coverage. A longer immersion in SBF (10 and 30 min) did not influence the relative intensity of the chitosan $(C_2H_6NO)^+$ fragment, but decreased the intensity of the $(C_2H_4NO)^+$ fragment. This reduced intensity of $(C_2H_4NO)^+$ could be the result of a more parallel orientation of CsA at low surface coverage after immersion for 10 and 30 min.

Overall, the greater yield of the $(C_2H_6NO)^+$ fragment after immersion in SBF for 3 min illustrates the chitosan layer covered by patchy CsA layer with polypeptide molecules oriented perpendicularly towards the chitosan underlayer. After immersion for 10 and 30 min, the CsA islands disappear, denoted by disappearance of the molecular ions. This indicates that a very small amount of CsA becomes oriented more parallel towards the chitosan layer. These findings clearly show that the chitosan layer is present at the PET_{air} surface after placing the biomaterial in SBF. This is particularly important in terms of improving and maintaining the biocompatibility of PET surfaces. However, the exact yield mechanism of the chitosan $(C_2H_4NO)^+$, $(C_2H_5NO)^+$ and $(C_2H_6NO)^+$ fragments under different immersion time of the chitosan/CsA layer is beyond the scope of this paper and requires more extensive studies.

The desorption of CsA from the biomaterial surface is related to the fact that CsA does not form chemical bonds with chitosan. Chitosan and CsA may interact via hydrogen bonds and/or Lifshitz–van der Waals forces. It is likely that in the untreated CsA layer, CsA molecules exist mainly in a closed conformation due to the surrounding hydrophobic environment provided by the chitosan backbone. However, immersion in SBF – and thus changing the environment to a polar one – favours the open conformation of CsA, which can then interact more strongly with SBF and weakly with the chitosan layer. This allows CsA to be desorbed from the surface of the biomaterial. The ability of CsA to change its conformation from closed to open depending on the nature of the environment enables its transport through the lipid bilayer according to the mechanism of passive diffusion [18, 19]. Such results are very promising for the design and development of new drug-release systems.

Modification of the PET surface with air plasma and biological films can significantly improve its biocompatibility and minimise side effects associated with the body's response to a foreign material. The presence of chitosan film provides an additional function, namely the controlled release of CsA, a strong immunosuppressant drug that is used to prevent implant rejection.

4. Conclusions

We used TOF-SIMS to analyse the chemical composition and the spatial distribution of molecules in the mixed chitosan and CsA layers. They were deposited by the Langmuir–Blodgett technique on the air plasma–activated PET surface and then immersed in SBF. We identified the most characteristic CsA and chitosan fragments in the time-of-flight secondary ion mass spectra before and after immersing the samples in SBF.The results confirmed the effective PET surface coverage with chitosan and CsA. The chitosan layer was presumably chemically bonded to the activated PET support. Meanwhile, CsA was physically adsorbed on the chitosan layer via hydrogen

bonding and/or Lifshitz van der Waals forces. In the SBF environment, CsA underwent gradual desorption into the bulk phase over time, as indicated by the decreased relative intensity of the $(C_6H_{14}N)^+$, $(C_{61}H_{108}N_{10}O_{12})^+$ and $(C_{62}H_{112}N_{10}O_{12})^+$ fragments. This process was likely due to a change from closed to open conformation of CsA. In effect, the initially well-ordered and packed structure of the CsA monolayer was no longer maintained exposing the chitosan layer. Consistently, there was a significant increase in the relative intensity of the most prominent chitosan fragment, $(C_2H_6NO)^+$, after immersion in SBF.

Our findings are satisfactory from the application point of view. The release of CsA from the PET/chitosan surface can ensure relatively easy delivery of this immunosuppressive drug to living cells directly from the implant surface. Simultaneously, the increased biocompatibility of the PET surface can be maintained due to its durable binding to the polysaccharide. Therefore, designing two-component layers as coatings for implants and/or stents may facilitate the release of CsA, eliminating the problem of its low bioavailability.

5. References

[1] Williams DF; (2019) Challenges with the development of biomaterials for sustainable tissue engineering. Front Bioeng Biotechnol 31, 127. **DOI:**10.3389/fbioe.2019.00127

[2] Jurak M, Wiącek AE, Ładniak A, Przykaza K, Szafran K; (2021) What affects the biocompatibility of polymers? Adv Colloid Interface Sci 294, 102451. **DOI:**10.1016/j.cis.2021.102451

[3] Song X, Tang Z, Liu W, Chen K, Liang J, Yuan B, Lin H, Zhu X, Fan Y, Shi X, Zhao P, Yang L, Zhang K, Mikos AG, Zhang X; (2022) Biomaterials and regulatory science. J Mater Sci Technol 128, 221–227. **DOI:**10.1016/j.jmst.2022.04.018

[4] Farhatnia, Y, Tan A, Motiwala A, Cousins BG, Seifalian AM; (2013) Evolution of covered stents in the contemporary era: clinical application, materials and manufacturing strategies using nanotechnology. Biotechnol Adv 31, 524–542. **DOI:**10.1016/ j.biotechadv.2012.12.010

[5] Li T, Ma K, Zhang T; (2022) UV-curable semi-interpenetrating matrix for polyester fabric-covered stents. Progr Org Coat 172, 107084. **DOI:**10.1016/j.porgcoat.2022.107084

[6] Jafernik K, Ładniak A, Blicharska E, Czarnek K, Ekiert H, Wiącek AE, Szopa A; (2023) Chitosan-based nanoparticles as effective drug delivery systems – a review. Molecules 28, 1963. **DOI:**10.3390/molecules28041963

[7] Pina S, Oliveira JM, Reis RL; (2015) Natural-based nanocomposites for bone tissue engineering and regenerative medicine: a review. Adv Mater 27, 1143–1169. **DOI:**10.1002/adma.201403354

[8] Rinaudo M; (2006) Chitin and chitosan: Properties and applications. Prog Polym Sci 31, 603–632. **DOI:**10.1016/j.progpolymsci.2006.06.001

[9] Ahmed S, Ikram S; (2016) Chitosan based scaffolds and their applications in wound healing. Achiev Life Sci 10, 27–37. **DOI:**10.1016/j.als.2016.04.001

[10] Carreira AS, Gonçalves FAMM, Mendonça PV, Gil MH, Coelho JFJ; (2010) Temperature and pH responsive polymers based on chitosan: applications and new graft copolymerization strategies based on living radical polymerization. Carbohydr Polym 80, 618–630. **DOI:**10.1016/j.carbpol.2009.12.047

[11] Li J, Cai C, Li J, Li J, Li J, Sun T, Wang L, Wu H, Yu G; (2018) Chitosan-based nanomaterials for drug delivery. Molecules 23, 2661. **DOI:**10.3390/molecules23102661

[12] Jang TS, Choen KH, Ahn JH, Song EH, Kim HE; (2019) *In-vitro* blood and vascular compatibility of sirolimus-eluting organic/inorganic hybrid stent coatings. Colloids Surf B Biointerfaces 179, 405–413. **DOI:**10.1016/j.colsurfb.2019.04.018

[13] Kersani D, Mugin J, Lopez M, Degoutin S, Tabary N, Cazaux F, Janus L, Maton M, Chai F, Sobocinski J, Blanchemain N, Martel B; (2020) Stent coating by electrospinning with chitosan/poly-cyclodextrin based nanofibers loaded with simvastatin for restenosis prevention. Eur J Pharm Biopharm 150, 156–167. **DOI:**10.1016/j.ejpb.2019.12.017

[14] Baldrick P; (2010) The safety of chitosan as a pharmaceutical excipient. Regul Toxicol Pharmacol 56, 290–299. **DOI:**10.1016/j.yrtph.2009.09.015

[15] Czogalla A; (2008) Oral cyclosporine A - the current picture of its liposomal and other delivery systems. Cell Mol Biol Lett 14, 139–152. **DOI:**10.2478/s11658-008-0041-6

[16] Tedesco D, Haragsim L; (2012) Cyclosporine: a review. J Transplant 2012, 230386. **DOI:**10.1155/2012/230386

[17] Wiącek AE, Jurak M, Ładniak A, Przykaza K, Szafran K; (2020) Cyclosporine CsA - The physicochemical characterization of liposomal and colloidal systems. Colloids Interfaces 4, 46. **DOI:**10.3390/colloids4040046

[18] Witek J, Keller BG, Blatter M, Meissner A, Wagner T, Riniker S; (2016) Kinetic models of cyclosporin A in polar and apolar environments reveal multiple congruent conformational states. J Chem Inf Model 56, 1547–1562. **DOI:**10.1021/acs.jcim.6b00251

[19] Dougherty PG, Sahni A, Pei D; (2019) Understanding cell penetration of cyclic peptides. Chem Rev 119, 10241–10287. **DOI:**10.1021/acs.chemrev.9b00008

[20] De Campos AM, Sánchez A, Alonso MJ; (2001) Chitosan nanoparticles: A new vehicle for the improvement of the delivery of drugs to the ocular surface. Application to cyclosporin A. Int J Pharm 224, 159–168. **DOI:**10.1016/S0378-5173(01)00760-8

[21] Philipova OE, Volkov EV, Sitnikova NL, Khokhlov AR; (2001) Two types of hydrophobic aggregates in aqueous solutions of chitosan and its derivative. Biomacromol 2, 483–490. **DOI:**10.1021/bm005649a

[22] Trombino S, Curcio F, Poerio T, Pellegrino M, Russo R, Cassano R; (2021) Chitosan membranes filled with cyclosporine A as possible devices for local administration of drugs in the treatment of breast cancer. Molecules 26, 1889. **DOI:**10.3390/molecules26071889

[23] Islama MM, Shahruzzamana M, Biswasa S, Sakiba MN, Rashida TU; (2020) Chitosan based bioactive materials in tissue engineering applications - a review. Bioact Mater 5, 164–183. **DOI:**10.1016/j.bioactmat.2020.01.012

[24] Kokubo T, Takadama H; (2006) How useful is SBF in predicting *in vivo* bone bioactivity? Biomaterials 27, 2907–2915. **DOI:**10.1016/j.biomaterials.2006.01.017

[25] Szafran K, Jurak M, Mroczka R, Wiącek AE; (2022) Surface properties of the polyethylene (PET) substrate modified with the phospholipid-polypeptide-antioxidant films: design of functional biocoatings. Pharmaceutics 14, 2815. **DOI:**10.3390/pharmaceutics14122815

[26] Szafran K, Jurak M, Mroczka R, Wiącek AE; (2023) Preparation and characterization of chitosan-based coatings for PET materials. Molecules 28, 2375. **DOI:**10.3390/molecules28052375

[27] Szafran K, Jurak M, Wiącek AE; (2022) Effect of chitosan on the interactions between phospholipid DOPC, cyclosporine A and lauryl gallate in the Langmuir monolayers. Colloids Surf A Physicochem Eng Asp 652, 129843. **DOI:**10.1016/j.colsurfa.2022.129843

[28] Pandiyaraj KN, Selvarajan V, Rhee YH, Kim HW, Shah SI; (2009) Glow discharge plasma-induced immobilization of heparin and insulin on polyethylene film surfaces enhances anti-thrombogenic properties. Mater Sci Eng C 3, 796–805. **DOI:**10.1016/j.msec.2008.07.013

[29] Bui V-T, Liu X, Ko SH, Choi H-S; (2015) Super-amphiphilic surface of nano silica/polyurethane hybrid coated PET film via a plasma treatment. J Colloid Interface Sci 453, 209–215. **DOI:**10.1016/j.jcis.2015.04.065

[30] Abdel-Fattah E; (2022) Surface modifications of PET in argon atmospheric pressure plasma: Gas flow rate effect. Surf Interface Anal 54, 794–802. **DOI:**10.1002/sia.7092

[31] McQuaw CM, Sostarecz AG, Zheng L, Ewing AG, Winograd N; (2005) Lateral heterogeneity of dipalmitoylphosphatidylethanolamine-cholesterol Langmuir-Blodgett films investigated with imaging time-of-flight secondary ion mass spectrometry and atomic force microscopy. Langmuir 21, 807–813. **DOI:**10.1021/la0479455

[32] Przykaza K, Jurak M, Wiącek AE, Mroczka R; (2021) Characteristics of hybrid chitosan/phospholipid-sterol, peptide coatings on plasma activated PEEK polymer. Mat Sci Eng C 120, 111658. **DOI:**10.1016/j.msec.2020.111658

[33] Finšgar M, Ristić T, Fardim P, Zemljič LF; (2018) Time-of-flight secondary ion mass spectrometry analysis of chitosan-treated viscose fibres. Anal Biochem 557, 131–141. **DOI:**10.1016/j.ab.2018.07.021

[34] Jurak M, Wiącek AE, Mroczka R, Łopucki R; (2017) Chitosan/phospholipid coated polyethylene terephthalate (PET) polymer surfaces activated by air plasma. Colloids Surf A Physicochem Eng Asp 532, 155–164. **DOI:**10.1016/j.colsurfa.2017.05.061

[35] Muddiman DC, Gusev AI, Stoppek-Langner K, Proctor A, Herkules DM, Tata P, Venkataramanan R, Diven W; (1995) Simultaneous quantification of cyclosporin A and its major metabolites by time-of-flight secondary-ion mass spectrometry and matrix-assisted laser desorption/ionization mass spectrometry utilizing data analysis techniques: Comparison with high-performance liquid chromatography. J Mass Spectrom 30, 1469–1479. **DOI:**10.1002/jms.1190301013

[36] Muddiman DC, Nicola AJ, Proctor A, Herkules DM; (1996) Important aspects concerning the quantification of biomolecules by time-of-flight secondary-ion mass spectrometry. Appl Spectrosc 50, 161–166. **DOI:**10.1366/0003702963906410

[37] Nicola AJ, Muddiman DC, Hercules DM; (1996) Enhancement of ion intensity in time-of-flight secondary-ionization mass spectrometry. JASMS 7, 467–472. **DOI:**10.1016/1044-0305(96)00006-2

[38] Biddulph GX, Piwowar AM, Fletcher JS, Lockyer NP, Vickerman JC; (2007) Properties of C_{84} and $C_{24}H_{12}$ molecular ion sources for routine TOF-SIMS analysis. Anal Chem 79, 7259–7266. **DOI:**10.1021/ac071442x

[39] Jurak M, Mroczka R, Łopucki R; (2018) Properties of artificial phospholipid membranes containing lauryl gallate or cholesterol. J Membr Biol 251, 277–294. **DOI:**10.1007/s00232-018-0025-z